

Crystal Structures of a Novel Ferric Reductase from the Hyperthermophilic Archaeon *Archaeoglobus fulgidus* and Its Complex with NADP⁺

Hsiu-Ju Chiu,* Eric Johnson,† Imke Schröder,†† and Douglas C. Rees†*

*Howard Hughes Medical Institute
Division of Chemistry and Chemical Engineering
147-75CH

California Institute of Technology
Pasadena, California 91125

†Department of Microbiology and Molecular Genetics
University of California, Los Angeles
Los Angeles, California 90095

Summary

Background: Studies performed within the last decade have indicated that microbial reduction of Fe(III) to Fe(II) is a biologically significant process. The ferric reductase (FeR) from *Archaeoglobus fulgidus* is the first reported archaeal ferric reductase and it catalyzes the flavin-mediated reduction of ferric iron complexes using NAD(P)H as the electron donor. Based on its catalytic activity, the *A. fulgidus* FeR resembles the bacterial and eukaryotic assimilatory type of ferric reductases. However, the high cellular abundance of the *A. fulgidus* FeR (~0.75% of the total soluble protein) suggests a catabolic role for this enzyme as the terminal electron acceptor in a ferric iron-based respiratory pathway [1].

Results: The crystal structure of recombinant *A. fulgidus* FeR containing a bound FMN has been solved at 1.5 Å resolution by multiple isomorphous replacement/anomalous diffraction (MIRAS) phasing methods, and the NADP⁺-bound complex of FeR was subsequently determined at 1.65 Å resolution. FeR consists of a dimer of two identical subunits, although only one subunit has been observed to bind the redox cofactors. Each subunit is organized around a six-stranded antiparallel β barrel that is homologous to the FMN binding protein from *Desulfovibrio vulgaris*. This fold has been shown to be related to a circularly permuted version of the flavin binding domain of the ferredoxin reductase superfamily. The *A. fulgidus* ferric reductase is further distinguished from the ferredoxin reductase superfamily by the absence of a Rossmann fold domain that is used to bind the NAD(P)H. Instead, FeR uses its single domain to provide both the flavin and the NAD(P)H binding sites. Potential binding sites for ferric iron complexes are identified near the cofactor binding sites.

Conclusions: The work described here details the structures of the enzyme-FMN, enzyme-FMN-NADP⁺, and possibly the enzyme-FMN-iron intermediates that are present during the reaction mechanism. This structural information helps identify roles for specific residues during the reduction of ferric iron complexes by the *A. fulgidus* FeR.

Introduction

Iron plays an essential metabolic role as a component of a diverse group of metalloproteins, as well as serving as an energy source in catabolic iron metabolism. While iron assimilation has been studied in many eukaryotic and prokaryotic organisms, dissimilatory iron respiration, a purely microbial feature, is not well understood. Respiration with Fe(III) is considered to be one of the earliest forms of energy-generating metabolism, well preceding the ability to respire with oxygen [2]. Due to the possible photochemical oxidation of Fe(II) in the Archaeal seas and the discharge of Fe(III) from hydrothermal vent fluids, Fe(III) was suggested to have been an abundant substrate on the early earth. Several hyperthermophilic, deep-branching Archaea and Bacteria have the demonstrated capability to reduce Fe(III), indicating that Fe(III) reduction was most likely a respiratory process of the last common ancestor.

Archaeoglobus fulgidus, a strictly anaerobic, hyperthermophilic archaeon [3], was found to reduce citrate-complexed Fe(III) [2]. *A. fulgidus* is a member of the *Archaeoglobales*, which constitute the only known sulfate-reducing archaea [4, 5]. Although growth with Fe(III) has not been demonstrated, the reduction of Fe(III) with H₂ gas is catalyzed by whole cells [2]. Recently, a highly active ferric reductase (FeR) was isolated from *A. fulgidus* [1]. It catalyzes the reduction of EDTA or citrate-complexed Fe(III) with either NADH or NADPH as the electron donor. The thermostable, homodimeric enzyme has a molecular mass of 18.7 kDa (169 residues) per subunit and lacks any prosthetic groups after purification. At elevated temperature, the enzyme can be reconstituted with FMN (flavin mononucleotide), suggesting that the *A. fulgidus* FeR enzyme is a flavoprotein. Similar to the bacterial ferric reductases, the *A. fulgidus* FeR requires flavin in the form of either FMN or FAD (flavin adenine dinucleotide) as a cofactor for Fe(III) reduction. Flavin can be used as a substrate when complexed Fe(III) is not present.

The *A. fulgidus* FeR is homologous to a family of NAD(P)H:flavin oxidoreductases that are involved in the oxidative degradation of aromatic compounds and hydrocarbons or in polyketide biosynthesis [1]. The NAD(P)H:flavin oxidoreductase family includes the flavin reductase components of several two-component monooxygenase enzymes such as 4-hydroxyphenylacetate (4-HPA) 3-monooxygenase from *E. coli* and enzymes that are involved in the biosynthesis of antibiotics such as antinorhodin, frenolicin, granaticin, and chlortetracycline. It has been shown that the *E. coli* HpaC (the reductase component of the 4-HPA 3-monooxygenase) can reduce Fe(III) with high activity [6], although ferric reductase activity has not been detected so far in the reductase component of any other monooxygenases in this family. Proteins with well-characterized ferric reductase

† To whom correspondence should be addressed (e-mail: dcrees@caltech.edu [D. C. R.], imkes@microbio.ucla.edu [I. S.]).

Key words: ferric reductase; flavoproteins; ferredoxin reductase superfamily; iron metabolism; NAD(P)H:flavin oxidoreductase

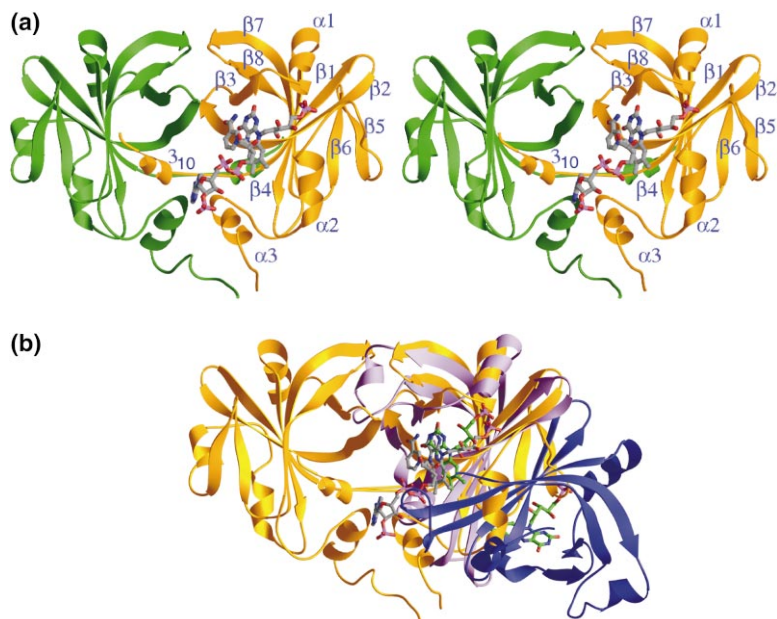


Figure 1. Ribbon Diagrams Illustrating the *A. fulgidus* FeR and the Comparison to the FMN-bp from *D. vulgaris*

(a) A stereoview of the FeR dimer viewed perpendicularly to the dimer two-fold axis (vertical). The FMN and NADP⁺ molecules are shown in ball-and-stick representation, with oxygen atoms in red, nitrogen atoms in blue, carbon atoms in gray, and phosphorus atoms in magenta. The secondary structural elements are labeled.

(b) Superposition of the A subunits of FeR and FMN-bp (PDB entry 1FLM), illustrating the different relationships between subunits in these dimeric proteins. Both FeR subunits are colored gold, and they are viewed from the same orientation as in Figure 1a. The two subunits of FMN-bp are colored magenta and blue, and the dimer two-fold axis is rotated ~42° clockwise in the plane of the page from the FeR dimer two-fold axis. The atom coloring of the cofactors is the same as in Figure 1a, with the cofactor bonds colored gray and green in FeR and FMN-bp, respectively.

activity, such as the *E. coli* flavin reductase (Fre) [7], which is a member of the ferredoxin reductase superfamily and is the major ferric reductase in the iron metabolism of *E. coli* [8], do not exhibit obvious sequence similarities to FeR.

To provide a molecular framework for characterizing the catalytic mechanism of ferric reductase, we have determined the three-dimensional structures of the recombinant *A. fulgidus* ferric reductase with a bound FMN at 1.5 Å resolution and in complex with NADP⁺ at 1.65 Å resolution. Unexpectedly, the *A. fulgidus* FeR adopts a polypeptide fold similar to the FMN binding protein (FMN-bp) from *Desulfovibrio vulgaris* Miyazaki F [9, 10]. This fold consists of a six-stranded antiparallel β barrel with a capping helix that interacts with the ribityl phosphate group of the flavin. Following the structure determination of FMN-bp, it was recognized that this β barrel is a circular permutation of the flavin binding domain of the ferredoxin reductase superfamily [11, 12]. The ferredoxin reductase superfamily has been extensively characterized, with structures available for the *E. coli* Fre [13]; ferredoxin:NADP⁺ reductase (FNR) from *Azotobacter vinelandii* [14], spinach leaf [15–17], pea [18], and cyanobacterium *Anabaena* [19]; flavodoxin reductase from *E. coli* [20]; porcine cytochrome *b₅* reductase [21]; nitrate reductase from corn [22, 23]; phthalate dioxygenase reductase from *Pseudomonas cepacia* [24]; and mammalian cytochrome P450 reductase [25]. Ferredoxin reductase-type proteins consist of two domains, an FAD or FMN binding domain organized around the six-stranded antiparallel β barrel and capping α helix, and a Rossmann fold NAD(P)H binding domain. In addition to the circular permutation of the β barrel, the *A. fulgidus* FeR distinguishes itself from members of the ferredoxin reductase family by the absence of the Rossmann fold domain and instead has an extension of two helices that provide binding sites for NAD(P)H. Thus, *A. fulgidus* FeR constitutes a new subclass of NAD(P)H binding enzymes.

Results and Discussion

Structure Description

The two subunits of the *A. fulgidus* FeR homodimer are related by a molecular two-fold rotation axis that is a noncrystallographic symmetry (NCS) operation in the FeR crystal. A ribbon diagram of the dimer viewed perpendicularly to this two-fold axis is shown in Figure 1a. The secondary structure, defined by PROCHECK [26], consists of eight β strands, three α helices, and a short 3_{10} helix as follows: residues 2–9 (3_{10}), 13–20 ($\beta 1$), 23–36 ($\beta 2$), 40–48 ($\beta 3$), 50–59 ($\alpha 1$), 61–68 ($\beta 4$), 72–81 ($\alpha 2$), 94–98 ($\beta 5$), 102–106 ($\beta 6$), 108–121 ($\beta 7$), 125–139 ($\beta 8$), and 146–155 ($\alpha 3$). A *cis* peptide bond involving Pro39 is located in the loop between $\beta 2$ and $\beta 3$. Each subunit consists of a central six-stranded antiparallel β barrel (with strand order $\beta 1$, $\beta 2$, $\beta 3$, $\beta 8$, $\beta 7$, and $\beta 4$) with a capping α helix ($\alpha 1$) flanked by $\alpha 2$, $\beta 5$, and $\beta 6$ on the lateral side and $\alpha 3$ and a 3_{10} helix on the bottom side. The two subunits are covalently linked by a disulfide bond between the Cys121 residues of each subunit. The remaining cysteines in each subunit, Cys25 and Cys45, form the mercury binding sites in both thiomersal and ethyl mercuric phosphate derivatives. Residue Phe33 of each subunit, located in $\beta 2$ at the dimer interface, adopts two conformations of 40:60 relative occupancies that pack against each other. Interestingly, only one of the subunits (subunit A) contains FMN, and NADP⁺ binds only to the subunit that is preoccupied with FMN. Soaking of native crystals in 10 mM FMN solutions failed to introduce FMN into subunit B, even though this site is free of intermolecular contacts that could block access. Likewise, soaking of native crystals in NADP⁺ solution only introduced NADP⁺ into subunit A, but not subunit B. The introduction of NADP⁺ did not perturb the preexisting interactions between FMN and the active site residues.

The structures of the native and the NADP⁺ complexes are very similar to each other, with an rmsd of 0.22 Å for residues 1–152 from both subunits A and B.

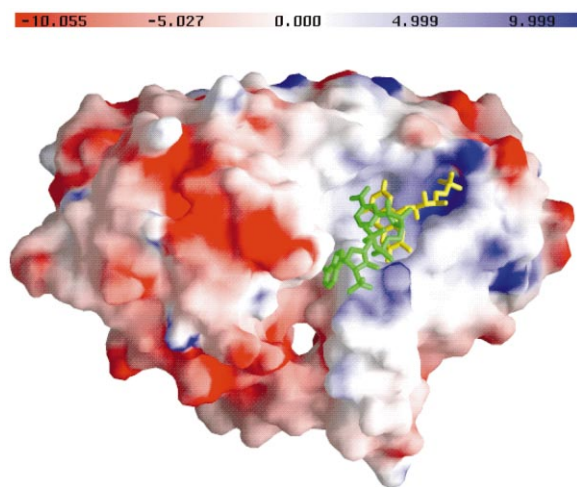


Figure 2. Binding Sites for the FMN and NADP⁺ Cofactors in a Positively Charged Groove Near the FeR Dimer Interface

The electrostatic potential of the *A. fulgidus* FeR dimer is mapped onto the solvent accessible surface, as calculated with the program GRASP [42]. The FMN and NADP⁺ molecules are shown in yellow and green, respectively. The color scheme for the electrostatic potential is indicated in units of kcal/mole/electron, with red and blue corresponding to negatively and positively charged surfaces, respectively.

In both the native and NADP⁺ complex structures, the major structural differences between the two subunits occur in two regions, a loop between residue 82 and 88 (involved in FMN binding) and the C-terminal residues 153–169 (involved in NADP⁺ binding). As a result of these differences, Arg160 from the A subunit of a neighboring molecule in the crystal sterically blocks the NADP⁺ binding site on the B subunit, while the A subunit binding site remains available for cofactor binding. Excluding residues 82–88 and 153–159, the rmsd in C α positions between the two subunits are 0.42 and 0.49 Å for the native and the NADP⁺ complex, respectively. The central β barrel is structurally conserved between the subunits in the dimer, with an rmsd of 0.23 and 0.28 Å for the native and the NADP⁺ complex, respectively.

A search with the program DALI [27] identified FMN-bp [9, 10] as the most structurally similar protein to FeR in the Protein Data Bank. Both proteins are organized around a common six-stranded antiparallel β barrel that binds flavin in similar fashions. A comparison of FMN-bp and FeR with the program LSQMAN [28] superimposed 74 residues in the two structures (of which 10 [13.5%] are identical), with an rmsd in C α positions of 1.93 Å. The fold is a circularly permuted version of the β barrel found in the flavin binding domains of the ferredoxin reductase superfamily [11, 12]. Despite this difference, the flavin binding sites of FeR/FMN-bp and ferredoxin reductase-type proteins are spatially equivalent. Members of the ferredoxin reductase superfamily have a second, Rossmann fold domain that is used to bind nicotinamide nucleotides; although NAD(P)H is a substrate for ferric reductases, this domain is absent in FeR.

The dimer interface in FeR is flat and involves both hydrophobic and hydrogen bonding interactions from the symmetrically packed β strands (β 2, β 3, β 7, and

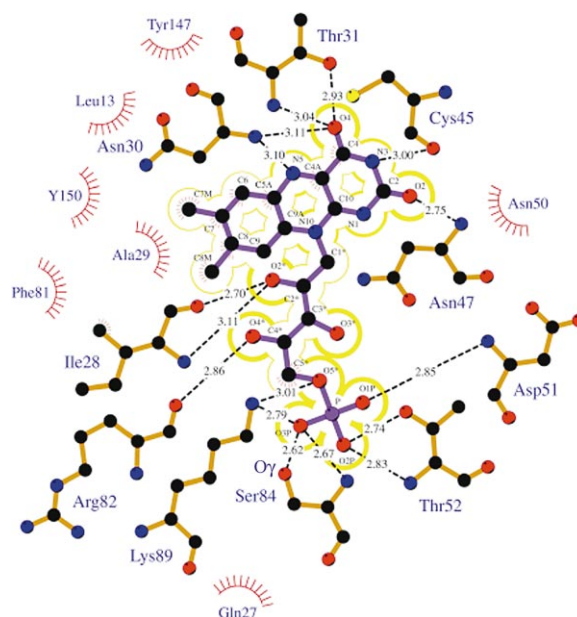


Figure 3. Interactions between the Active Site Residues and FMN in FeR

The solvent accessibility of the FMN is indicated by the intensity of the yellow shading around each atom, with the brighter colors representing more solvent accessible atoms. The solvent accessibility of FMN is calculated from the NADP⁺-free structure. The figure was generated using LIGPLOT [43].

β 8), the N-terminal 3_{10} helix, and the C-terminal residues 158–169. The N-terminal 3_{10} helix and the first part of β 1 run antiparallel to each other and cross the dimer interface to interact with β 7 and β 8 in the neighboring subunit. The accessible surface areas for subunit A, B, and the entire dimer are 9,050, 9,900, and 14,450 Å², respectively, resulting in a buried surface area of \sim 4,500 Å² per dimer. While the crystal structure of FMN-bp also revealed a dimeric organization for this homolog of FeR, the subunit-subunit interactions are quite distinct from those observed in FeR (Figure 1b). In FMN-bp, the dimer interface involves residues located in regions equivalent to β strands β 1, β 2, β 4, and β 7 of FeR. When one subunit of FeR and FMN-bp are superimposed, the two-fold axes of these dimeric proteins are tilted with respect to each other by \sim 42° and displaced to opposite sides of the β barrel.

FMN Binding Site

FMN is bound in a groove near the dimer interface (Figure 2). The groove is surrounded by the α 1, α 2, and α 3 helices, the β 2 strand, and an N-terminal 3_{10} helix. The FMN lies on the edge of the β strand plane containing the β 1, β 2, β 4, β 7, and β 8 strands, such that the plane of the isoalloxazine ring is perpendicular to the plane of these β strands. The 2,4-pyrimidinedione (uracil) moiety of the isoalloxazine ring contacts the β 2 and β 3 strands. The dimethylbenzene edge of the isoalloxazine ring is located between the α 2 and α 3 helices and is surrounded by hydrophobic residues Leu13, Ile28, Phe81, Tyr147, and Tyr150. The *si* face of the isoalloxazine is buried and contacts the β 2 strand. The ribityl phosphate

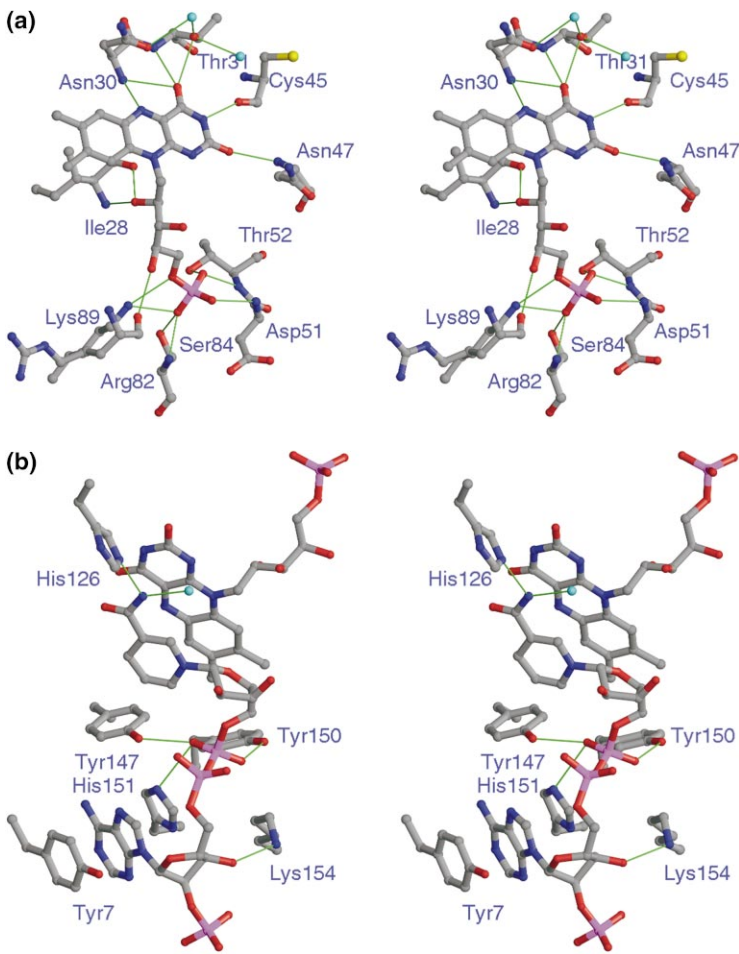


Figure 4. Stereoview of the FMN and NADP⁺ Binding Sites in *A. fulgidus* FeR
Atoms are colored according to the scheme in Figure 1.

group of FMN runs along the edge of β strands, interacting with the $\beta 2$ strand and wedging between the $\alpha 1$ and $\alpha 2$ helices. The phosphate group is positioned at the N terminus of the short α helix ($\alpha 1$) that caps the β barrel. In addition to the positive electrostatic dipole provided by the capping helix, the FMN is stabilized by 15 hydrogen bonds and 1 ion pair interaction (Figures 3 and 4a). Eleven of these sixteen interactions involve main chain atoms (N or O), while the remaining five are

from side chain atoms (Thr, Ser, and Lys) of the active site residues. It is noticeable that the majority of the residues involved in the FMN binding in the *A. fulgidus* FeR structure are not conserved in sequences of FeR homologs; many of these residues (although not all) interact with FMN through main chain N or O atoms. Excluding N1 and O3*, every N or O atom of the FMN forms at least one hydrogen bond to the surrounding residues. Computer docking of FAD onto the FMN

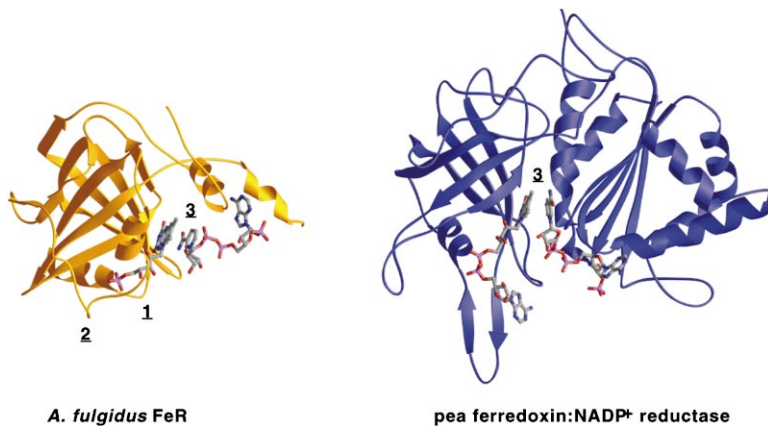


Figure 5. Comparison of *A. fulgidus* FeR and Pea FNR, Illustrating the Major Structural Differences between FeR and Members of the Ferredoxin Reductase Superfamily

The two structures are depicted on the same scale and are viewed in equivalent orientations, with FeR on the left, and pea FNR ([18]; PDB entry 1QFY) on the right. The Rossmann domain in FNR is replaced by two helices in FeR. The regions in the flavin binding domain that differ between FeR and FNR are identified by numbers in the figure.

- (1) The loop between the $\alpha 1$ and the $\beta 3$ is shorter in FeR.
- (2) FeR has a loop between $\alpha 2$ and $\beta 5$ that is involved in FMN phosphate binding.
- (3) The NMN portion of NADP⁺ in FeR is flipped by $\sim 180^\circ$ relative to the NADP⁺ in the 1QFY structure of pea FNR.

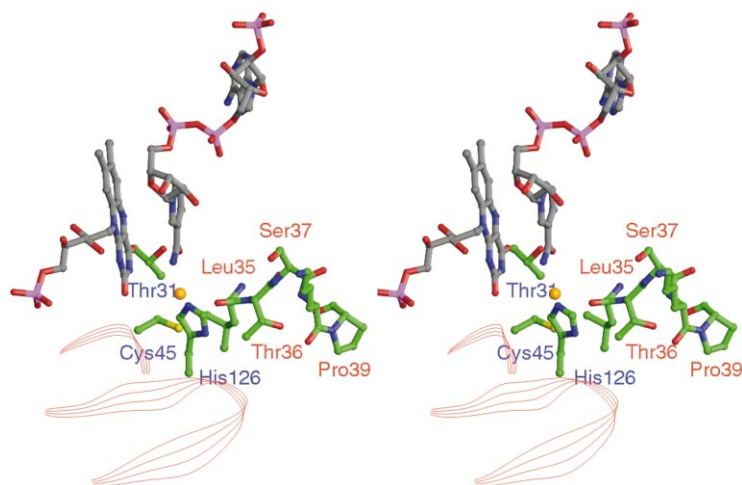


Figure 6. Stereoview of the Mercury Binding Site, Colored Gold, of the Thiomerical Derivative That is Located Near the Flavin of Subunit A in the *A. fulgidus* FeR

As discussed in the text, this site represents one of the putative binding sites on FeR for ferric iron complexes. The NADP⁺ is superimposed from the structure of NADP⁺ complex solved in the absence of the mercurial derivative. The labels for residues in the A and B subunits are colored blue and red, respectively.

shows that there is sufficient space in FeR to accommodate the AMP moiety of an FAD molecule, consistent with the observation that FeR can utilize either FMN or FAD for Fe³⁺ reduction.

The binding mode of FMN is similar in all of the members of the ferredoxin reductase family (Figure 5). The *si* face of the isoalloxazine ring is in contact with the β barrel, with the FMN phosphate anchored to the start of the capping helix α 1. Hydrogen bonding interactions between the protein and the isoalloxazine ring involve structurally similar residues in the β 2 and β 3 strands and the α 1 helix. There are two general structural distinctions between *A. fulgidus* FeR and other members of the family in the flavin binding domain (Figure 5). First, a loop between α 1 and β 3 in the *A. fulgidus* FeR is much shorter than the corresponding loop in the other FAD-bound superfamily members. Second, the *A. fulgidus* FeR has an extra loop of 12 residues (82–93) between α 2 and β 5, which is involved in FMN binding. The first part of this loop interacts with the FMN phosphate group in subunit A and is disordered in subunit B, where there is no FMN molecule bound. There are also differences in the detailed FMN-protein interactions between *A. fulgidus* FeR and the other members. For example, several residues involved in FMN binding that are conserved in other members of the superfamily are not found in FeR, including an Arg residue that interacts with the ribityl phosphate, a Tyr residue in contact with the *re* face of the isoalloxazine ring, and a Ser/Thr located near the edge of the isoalloxazine ring that is part of a conserved RXY(S/T) fingerprint sequence that has been recognized as a FAD/FMN binding motif in other flavoproteins [14].

NADP⁺ Binding Site

NADP⁺ is bound in a cleft between the FMN and the α 3 and 3_{10} helices. The NMN (nicotinamide mononucleotide) half of NADP⁺ is packed against the isoalloxazine ring of FMN, while the 2'-P-AMP half is extended outward between the N-terminal 3_{10} and α 3 helices. The nicotinamide ring of NADP⁺ binds to the *re* face of the central ring of the FMN isoalloxazine and packs at an angle of $\sim 15^\circ$ to the flavin isoalloxazine ring. The C4 of the nicotinamide and the N5 atom of FMN are 3.8 Å

apart, in an arrangement that is typical for direct hydride transfer in flavoproteins [29]. The N7 atom of nicotinamide is hydrogen bonded to His126 N ϵ 2, while the NMN phosphate interacts with Tyr147 O η , Tyr150 O η , and His151 N ϵ 2. His126 is conserved in all presently known homologs of FeR. The adenine ring of the 2'-P-AMP half is packed between Tyr7 and His151. The 2'-phosphate of the 2'-P-AMP faces the surface and contacts no protein residues, which is consistent with the observation that FeR can utilize either NADPH or NADH as an electron donor for Fe³⁺ reduction.

The structure of FeR complexed with NADP⁺ directly illustrates how nicotinamide interacts with the isoalloxa-

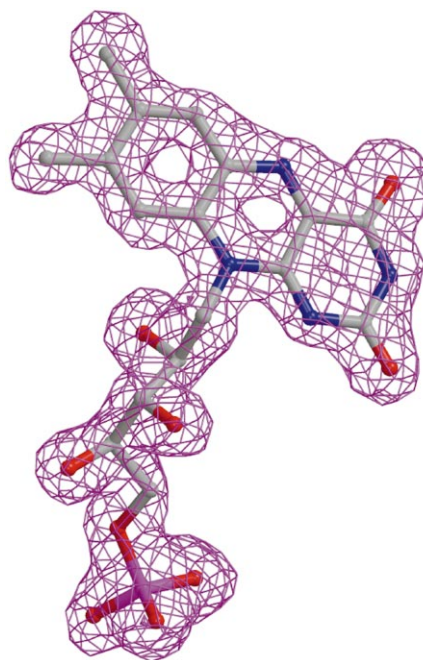


Figure 7. The 1.5 Å Resolution Experimental Phase-Extended Electron Density Map Surrounding the FMN

This map was calculated using data between 20 and 1.5 Å resolution and is contoured at 1.2 σ .

Table 1. Statistics for Data Collection and Heavy-Atom Phasing

	Native	NADP	Thiomersal	EMP ^a
Resolution (Å)	1.5	1.65	3.0	2.8
Wavelength (Å)	0.98	0.98	1.54	1.54
Total observations	286,113	168,005	54,389	55,834
Unique reflections	52,239	36,289	7,381	8,002
Completeness (%) ^b	92.0 (66.1)	86.1 (86.5)	99.3 (99.2)	88.2 (85.6)
R _{sym} (%) ^{b,c}	5.4 (33.9)	5.4 (20.4)	9.0 (20.4)	7.9 (19.4)
Phasing power ^d				
Centric			2.29	2.52
Acentric			3.57	3.65
R-cullis ^e				
Centric (isomorphous)			0.46	0.43
Acentric (isomorphous/anomalous)			0.41/0.76	0.41/0.72
Number of Hg sites			4	4
Overall FOM ^f			0.72	
FOM (DM/phase extension)			0.82	

^a EMP, ethyl mercuric phosphate.

^b Values in the parentheses correspond to the highest resolution shell (1.55–1.50 Å for native, 1.71–1.65 Å for NADP complex, 2.9–2.8 Å for ethyl mercuric phosphate derivative, and 3.11–3.0 Å for thiomersal derivative).

^c $R_{sym} = \sum_{hkl, l} [(\sum_i |I_{hkl, l} - \langle I_{hkl} \rangle|)] / \sum_{hkl, l} \langle I_{hkl} \rangle$, where the I_{hkl} is the intensity of an individual measurement of the reflection with indices hkl , and $\langle I_{hkl} \rangle$ is the mean intensity of that reflection.

^d Phasing power is the rms heavy-atom structure factor amplitude divided by the rms lack of closure.

^e $R_{cullis} = \sum ||F_{PH} - F_P| - F_H| / \sum |F_{PH} - F_P|$, where F_H is the calculated heavy-atom structure-factor amplitude, and F_P and F_{PH} are the native and derivative structure-factor amplitudes, respectively.

^f FOM, figure of merit.

zine ring in a wild-type member of the ferredoxin reductase superfamily, particularly concerning the details of the stacking interactions between the nicotinamide and isoalloxazine groups expected for this type of hydride transfer reaction. From the crystal structure of *A. fulgidus* FeR, the *re* face of the isoalloxazine of the FMN is completely open; therefore, the isoalloxazine ring is accessible for the nicotinamide binding in the soaking experiment. In other members of the ferredoxin reductase superfamily, it has not yet been possible to obtain productive NADP⁺ complexes by direct soaking of the wild-type protein, presumably because many of these other proteins have an aromatic residue from the C terminus of the NADPH domain stacked against, and cov-

ering, the isoalloxazine ring. The presence of this stacking residue has been proposed to protect the flavin from side reactions and to modulate the binding affinity of the protein for the nicotinamide cofactor [18]. Before productive interaction between the nicotinamide and flavin can take place, this aromatic residue would need to move away [18]. Recently, the stacking residue W308 of pea FNR was replaced with serine in the W308S mutant to obtain the structures for the complexes with NADP⁺ and NADPH [18]. In these structures, the nicotinamide ring packs against the isoalloxazine ring at an angle of ~30°, with the C4 atom 3 Å from the flavin N5 atom. The NADP⁺ molecule is bound in an orientation flipped 180° relative to the NADP⁺ molecule in *A. fulgidus* FeR (Figure 5).

Table 2. Refinement Statistics

	Native	NADP ⁺
Resolution range (Å)	20–1.5	20–1.65
Reflections	50,566	35,546
R/R _{free} (%) ^a	20.5/21.9	19.1/21.5
Number of residues	1–161/1–168	1–161/1–168
Number of water	227	237
Number of FMN	1	1
Number of NADP		1
Average B factor (Å ²)		
Protein	26.2	19.5
Water	32.6	26.9
FMN	12.6	8.7
NADP		28.3
Ramachandran plot (%) ^b		
Most favored/additional	93.7/6.3	93.5/6.5
Rmsd from idea values		
Bond length (Å)	0.011	0.008
Bond angle (°)	1.44	1.42

^a R_{free} is defined as R for 5% of the data omitted from the refinement.

^b Most favored, additional, generally allowed, and disallowed regions are defined by PROCHECK [26].

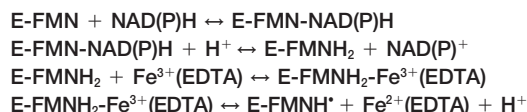
Potential Fe³⁺ Binding Sites

Ferric iron complexes could not be detected bound to *A. fulgidus* FeR, either directly through soaking experiments with Fe³⁺(EDTA) or indirectly through inspection of the electron density maps for the FMN and NADP⁺-bound structures (data not shown). It is possible that ferric complexes interact with the flavin near the exposed dimethylbenzene moiety, as seen in other flavo-proteins that participate in electron transfer processes [30]. A second potential ferric complex binding site is suggested by the binding site for organomercurials used in the structure determination. One of the four mercury sites is located in a pocket, formed by His126 Nε2, Cys45 Sγ, Leu35 O, and Thr31 Oγ, that sits near the edge of the 2,4-pyrimidinedione moiety of the flavin (Figure 6). The His126 residue is completely conserved, and the Cys45 residue is conserved as Cys/Ser among the 18 known homologs of *A. fulgidus* FeR [1]. Furthermore, residues 36–39 (T/SXXP), one of the three highly conserved regions in these sequences, are positioned near

this mercury binding site on the other subunit. This Hg atom is replaced by a water molecule in the structures of the native (W39, B = 25 Å²) and the NADP⁺ complex (W19, B = 15 Å²). Neither the phosphate group of the ethyl mercury phosphate derivative nor the thiosalicylate of the thiomersal derivative are observed in electron density maps that might indicate how the ligands of ferric complexes interact with FeR. The Hg site is located 6.0 Å and 6.3 Å from the N1 and N5 atoms, respectively, of the isoalloxazine ring.

Proposed Catalytic Mechanism

Since the affinity of FeR for FMN (~0.3 μM) is much greater than for NAD(P)H or ferric complexes such as Fe³⁺-EDTA (>~60 μM), it is likely that the reaction mechanism proceeds through an enzyme-bound flavin species [1]. A possible reaction mechanism consists of the following sequence:



The E-FMNH* species could subsequently reduce a second ferric complex or disproportionate to yield fully oxidized and reduced flavins. The work described in this paper provides structures of the E-FMN and the E-FMN-NADP⁺ complexes that represent two of the intermediates present in the reaction mechanism. Two potential binding sites for the ferric iron complexes are identified at opposing ends of the isoalloxazine ring; one is near the dimethylbenzene group, and the other is near the N3 position. The latter position was occupied by a mercury in a heavy-atom derivative, and assuming this reflects the ferric iron binding site, it appears that there would be insufficient space near the isoalloxazine ring to simultaneously accommodate both the Fe³⁺(EDTA) and nicotinamide. In this case, binding of these two substrates would be mutually exclusive. The structural information suggests an ordered reaction mechanism by which NAD(P)H binds to the active site, reduces FMN, and is released. Subsequently, complexed Fe³⁺ binds to the proposed metal binding site, where it receives its electron from the reduced FMN. Whether only half of the subunits of FeR are catalytically competent and capable of substrate binding, as suggested by the crystallographic studies, remains an open question and will require future studies addressing the kinetics and mechanism of this reaction.

Biological Implications

A. fulgidus FeR is a small protein that catalyzes the flavin-mediated electron transfer from NADPH to Fe³⁺. It is homologous to the FMN binding protein of *D. vulgaris* [9, 10], which is a circularly permuted variant of the antiparallel β barrel found in the flavin binding domain of members of the ferredoxin reductase superfamily. Each subunit in the FeR homodimer consists of a single domain that provides both flavin and NADPH binding sites. Compared to other proteins in the ferredoxin reductase superfamily, the structural design of *A. fulgidus* FeR

provides one of the simplest solutions for solving a similar enzymatic problem. Perhaps because of the anaerobic environment of *A. fulgidus*, there is no need for an aromatic residue to stack against the isoalloxazine ring to protect the reduced flavin from being oxidized by O₂, and the Rossmann fold domain used to bind the nicotinamide cofactors in other members of this superfamily has been replaced by two helices in FeR.

Experimental Procedures

Crystallization and Preparation of Heavy-Atom Derivatives

Purification and characterization of wild-type *A. fulgidus* FeR has been reported previously [1]. The recombinant protein used in the structural work was overexpressed in *E. coli* (E. J. and I. S., unpublished data). The crystals of the homodimeric enzyme were grown at 4°C by the hanging drop vapor diffusion technique, with protein solution at a concentration of 25 mg/ml in 0.1 M Tris-HCl (pH 7.5) and a reservoir consisting of 21%–22% w/v PEG4000, 0.1 M sodium acetate, and 0.1 M Tris-HCl (pH 8.4). The crystallization drops were microseeded after 20–24 hr. Rectangular plate-like crystals of dimensions 0.5 mm × 0.3 mm × 0.1 mm grew in 3–4 days. The crystals belong to space group P4₂2 with unit cell parameters a = b = 56.4 Å and c = 214.6 Å and contain one homodimer per asymmetric unit. A search for heavy-atom binding produced two mercury derivatives by soaking native crystals in the following conditions: 5 mM thiomersal or 2 mM ethyl mercury phosphate in 30% w/v PEG4000, 0.1 M sodium acetate, 0.1 M Tris-HCl (pH 8.4), and 10% glycerol at 20°C over 1–2 days, followed by back-soaking the derivatized crystals in the native mother liquor for 2 hr. The NADP⁺ complex was prepared by soaking the native crystals in 10 mM NADP⁺, 30% w/v PEG4000, 0.1 M sodium acetate, and 0.1 M Tris-HCl (pH 8.4) at 4°C overnight.

Data Collection

All diffraction data were collected under cryogenic conditions at 100K. Glycerol (20%) was added to the normal crystallization solution as a cryoprotectant. The crystals were soaked in this cryoprotectant solution for about 2 min, before being flash frozen directly in the cold nitrogen stream. The native data were measured at the Stanford Synchrotron Radiation Laboratory (SSRL) BL-9-2 using an ADSC Quantum 4 CCD detector, while the NADP⁺ complex data were collected at SSRL BL-9-1 using MAR image plate. The data for the two mercury derivatives were collected on an R-AXIS IV image plate scanner using Cu-Kα radiation from a Rigaku rotating anode generator. Data were processed with the programs DENZO and SCALEPACK [31].

Structure Solution and MIRAS Phasing

Four heavy-atom positions for each of the mercury derivatives were identified by the direct methods program *SnB* [32]. All of the mercury derivative data were postprocessed using the program DREAR [33] to generate the normalized difference structure factor amplitudes (diffE values) from the anomalous differences, which were then used by *SnB* to find the Hg positions. The 200 largest diffE values were used to generate 2000 triplet invariants. A total of 500 random trials were performed, and in each trial, 20 cycles of the *SnB* procedure were used to refine the phases. The results from the 500 trials clearly showed a bimodal distribution of *SnB* solutions with respect to the final minimal function value and indicated that 9 of the random trials had converged to a R_{min} value of ~0.38. Each of these nine solutions consistently showed four mercury sites. The thiomersal and ethyl mercury phosphate derivatives shared four common sites, which were later shown to be Cys25 and Cys45 in each monomer. The heavy-atom positions and occupancies were refined against both the anomalous and isomorphous differences to 2.8 Å resolution using the program MLPHARE [34]. The MIRAS phasing had an overall figure of merit (FOM) of 0.72 for reflections between 20–2.8 Å resolution. The MIRAS phases were further improved by solvent flattening with a solvent content of 42%, histogram matching, and phase extension to 1.5 Å resolution over 400 density modification cycles using DM [35]. The resulting electron density was of excellent

quality, revealing, for example, the bound FMN with holes in the isoalloxazine ring (Figure 7). A summary of the data collection and MIRAS phasing statistics is presented in Table 1.

Model Building and Refinement

The program wARP [36] was used for automatic model building. Following standard protocol suggested by the program, a total of 290 residues were traced over 6 hours in four chains that included residues 2–36 and 39–155 of subunit A and residues 2–69 and 90–150 of subunit B. All the side chains for these residues were then docked unambiguously into the sequence. The rest of the model was built manually using the program O [37]. All stages of refinement were carried out using the program CNS [38]. A bulk solvent correction and an overall anisotropic scaling were applied to the diffraction data. Several rounds of refinement and manual rebuilding resulted in a final R factor of 20.5% ($R_{\text{free}} = 21.9\%$) for all the data between 20 and 1.5 Å. The final model contains residues 1–161 and a bound FMN in subunit A, residues 1–168 in subunit B, and a total of 227 water molecules.

Residues 1–150 of each subunit in the native FeR model were used as a starting model for the NADP⁺ complex structure. The model was refined with the data between 20–1.65 Å resolution with a bulk solvent correction and an overall anisotropic B factor scaling applied using the program CNS. Several cycles of rigid body, simulated annealing, and individual B factor refinement resulted in a final R factor of 19.1% ($R_{\text{free}} = 21.5\%$). The final model consisted of residues 1–161, a bound FMN, and a bound NADP⁺ in subunit A, residues 1–168 in subunit B, and a total of 237 water molecules. Based on planarity of the ring systems, the FMN and NADP⁺ cofactors in these structures are in the oxidized state. PROCHECK [26] analysis of both structures showed that all residues were in either the most favored or additionally allowed regions of the Ramachandran plot. The final refinement statistics are summarized in Table 2.

Figure Preparation

Figures were prepared using RIBBONS v3.0 [39], MOLSCRIPT [40], RASTER3D [41], GRASP v1.25 [42], and LIGPLOT [43].

Acknowledgments

We thank the reviewers for their insightful comments. This work was supported by National Institutes of Health HL-16251 (I. S.) and National Institutes of Health GM-45162 (D. C. R). This work is based on research conducted at the Stanford Synchrotron Radiation Laboratory (SSRL), which is funded by the Department of Energy, Office of Basic Energy Sciences, and the National Institutes of Health.

Received: December 18, 2000

Revised: January 31, 2001

Accepted: February 20, 2001

References

- Vadas, A., Monbouquette, H.G., Johnson, E., and Schröder, I. (1999). Identification and characterization of a novel ferric reductase from the hyperthermophilic archaeon *Archaeoglobus fulgidus*. *J. Biol. Chem.* *274*, 36715–36721.
- Vargas, M., Kashefi, K., Blunt-Harris, E.L., and Loveley, D.R. (1998). Microbiological evidences for Fe(III) reduction on early earth. *Nature* *395*, 65–67.
- Stetter, K.O., et al., and Vance, I. (1993). Hyperthermophilic archaea are thriving in deep north-sea and Alaskan oil-reservoirs. *Nature* *365*, 743–745.
- Zellner, G., et al., and Winter, J. (1989). Isolation and characterization of thermophilic, sulfate reducing archaeobacterium *Archaeoglobus fulgidus* strain Z. *Syst. Appl. Microbiol.* *11*, 151–160.
- Stetter, K.O. (1988). *Archaeoglobus fulgidus* gen-Nov, sp-Nov – A new taxon of extremely thermophilic archaeobacteria. *Syst. Appl. Microbiol.* *10*, 172–173.
- Galan, B., Diaz, E., Prieto, M.A., and Garcia, J.L. (2000). Functional analysis of the small component of the 4-hydroxyphenylacetate 3-monooxygenase of *Escherichia coli* W: a prototype of a new flavin:NAD(P)H reductase subfamily. *J. Bacteriol.* *182*, 627–636.
- Spyrou, G., Haggard-Ljungquist, E., Krook, M., Jorvall, H., Nilsson, E., and Reichard, P. (1991). Characterization of the flavin reductase gene (Fre) of *Escherichia coli* and construction of a plasmid for overproduction of the enzyme. *J. Bacteriol.* *182*, 627–636.
- Coves, J., and Fontecave, M. (1993). Reduction and mobilization of iron by a NAD(P)H-flavin oxidoreductase from *Escherichia coli*. *Eur. J. Bacteriol.* *211*, 635–641.
- Liepinsh, E., Kitamura, M., Murakami, T., Nakaya, T., and Otting, G. (1997). Pathway of chymotrypsin evolution suggested by the structure of the FMN-binding protein from *Desulfovibrio vulgaris* (Miyazaki F). *Nat. Struct. Biol.* *4*, 975–979.
- Suto, K., et al., and Yasuoka, N. (2000). How do the X-ray structure and the NMR structure of FMN-binding protein differ? *Acta Crystallogr. D56*, 368–371.
- Murzin, A.G. (1998). Probable circular permutation in the flavin-binding domain. *Nat. Struct. Biol.* *5*, 101.
- Liepinsh, E., Kitamura, M., and Murakami, T. (1998). Common ancestor of serine proteases and flavin-binding domains. *Nat. Struct. Biol.* *5*, 102–103.
- Ingelman, M., Ramaswamy, S., Niviere, V., Fontecave, M., and Eklund, H. (1999). Crystal structure of NAD(P)H:flavin oxidoreductase from *Escherichia coli*. *Biochemistry* *38*, 7040–7049.
- Prasad, G.S., et al., and Stout, C.D. (1998). The crystal structure of NADPH:ferredoxin reductase from *Azotobacter vinelandii*. *Protein Sci.* *7*, 2541–2549.
- Karplus, P.A., Daniels, M.J., and Herriott, J.R. (1991). Atomic structure of ferredoxin-NADP⁺ reductase: prototype for a structurally novel flavoenzyme family. *Science* *251*, 60–66.
- Bruns, C.M., and Karplus, P.A. (1995). Refined crystal structure of spinach ferredoxin reductase at 1.7 Å resolution: oxidized, reduced and 2'-phospho-5'-AMP bound states. *J. Mol. Biol.* *247*, 125–145.
- Aliverti, A., et al., and Zanetti, G. (1995). Involvement of serine 96 in the catalytic mechanism of ferredoxin-NADP⁺ reductase: structure–function relationship as studied by site-directed mutagenesis and X-ray crystallography. *Biochemistry* *34*, 8371–8379.
- Deng, Z., et al., and Karplus, P.A. (1999). A productive NADP⁺ binding mode of ferredoxin-NADP⁺ reductase revealed by protein engineering and crystallographic studies. *Nat. Struct. Biol.* *6*, 847–853.
- Serre, L., Vellieux, F.M.D., Medina, M., Gomez-Moreno, C., Fontecilla-Camps, J.C., and Frey, M. (1996). X-ray structure of the ferredoxin:NADP(+) reductase from cyanobacterium *Anabaena PCC 7119* at 1.8 Å resolution, and crystallographic studies of NADP(+) binding at 2.25 Å resolution. *J. Mol. Biol.* *263*, 20–39.
- Ingelman, M., Bianchi, V., and Eklund, H. (1997). The three-dimensional structure of flavodoxin reductase from *Escherichia coli* at 1.7 Å resolution. *J. Mol. Biol.* *268*, 147–157.
- Nishida, H., Inaka, K., Yamanaka, M., Kaida, S., Kobayashi, K., and Miki, K. (1995). Crystal structure of NADH cytochrome b5 reductase from pig liver at 2.4 Å resolution. *Biochemistry* *34*, 2763–2767.
- Lu, G.G., Campbell, W.H., Schneider, G., and Lindqvist, Y. (1994). Crystal structure of the FAD containing fragment of corn nitrate reductase at 2.5 Å resolution—relationship to other flavo-protein reductases. *Structure* *2*, 809–821.
- Lu, G.G., Lindqvist, Y., Schneider, G., Dwivedi, U., and Campbell, W. (1995). Structural studies on corn nitrate reductase: refined structure of the cytochrome b reductase fragment at 2.5 Å, its ADP complex and an active-site mutant and modeling of the cytochrome b domain. *J. Mol. Biol.* *248*, 931–948.
- Correll, C.C., Batie, C.J., Ballou, D.P., and Ludwig, M.L. (1992). Phthalate dioxygenase reductase: a modular structure for electron transfer from pyridine nucleotides to [2Fe-2S]. *Science* *258*, 1604–1610.
- Wang, M., Roberts, D.L., Paschke, R., Shea, T.M., Masters, B.S., and Kim, J.J. (1997). Three-dimensional structure of NADPH-cytochrome P450 reductase: prototype for FMN- and FAD-containing enzymes. *Proc. Natl. Acad. Sci. USA* *94*, 8411–8416.
- Laskowski, R.A., McArthur, M.W., Moss, D.S., and Thornton, J.M. (1993). A simple method for assessing the quality of protein structure: the WHATCHECK program. *J. Mol. Biol.* *233*, 147–157.

- J.M. (1993). PROCHECK - a program to check the stereochemical quality of protein structures. *J. Appl. Cryst.* **26**, 283–291.
27. Holm, L., and Sander, C. (1993). Protein structure comparison by alignment of distance matrices. *J. Mol. Biol.* **233**, 123–138.
 28. Kleywegt, G.J., and Jones, T.A. (1997). Detecting folding motifs and similarities in protein structures. *Methods Enzymol.* **277**, 525–545.
 29. Fraaije, M.W., and Mattevi, A. (2000). Flavoenzymes: diverse catalysts with recurrent features. *Trends Biochem. Sci.* **25**, 126–132.
 30. Massey, V. (1995). Introduction: flavoprotein structure and mechanism. *FASEB J.* **9**, 473–475.
 31. Otwinowski, Z., and Minor, W. (1997). Processing of x-ray diffraction data collected in oscillation mode. *Methods Enzymol.* **276**, 307–326.
 32. Weeks, C.M., and Miller, R. (1999). The design and implementation of SnB version 2.0. *J. Appl. Crystallogr.* **32**, 120–124.
 33. Blessing, R.H., and Smith, G.D. (1999). Difference structure factor normalization for heavy atom or anomalous scattering substructure determinations. *J. Appl. Crystallogr.* **32**, 664–670.
 34. Otwinowski, Z. (1991). Maximum likelihood refinement of heavy atom parameters. In *Isomorphous Replacement and Anomalous Scattering*. W. Wolf, P.R.E Evans, and A.G. Leslie, eds. (Warrington, UK: Daresbury Laboratory), pp. 80–86.
 35. Cowtan, K. (1994). An automated procedure for phase improvement by density modification. *Joint CCP4 ESF-EACBM Newsletter. Protein Crystallogr.* **31**, 34–38.
 36. Perrakis, A., Moras, R., and Lamzin, V.S. (1999). Automated protein model building combined with iterative structure refinement. *Nat. Struct. Biol.* **6**, 458–463.
 37. Jones, T.A., Zhou, J.Y., Cowan, S.W., and Kjeldgaard, M. (1991). Improved methods for building protein models in electron density maps and the location of errors in these models. *Acta Crystallogr.* **A47**, 110–119.
 38. Brunger, A., et al., and Warren, G. (1998). Crystallography & NMR system: A new software suite for macromolecular structure determination. *Acta Crystallogr. D* **54**, 905–921.
 39. Carson, M. (1991). RIBBONS 2.0. *J. Appl. Crystallogr.* **24**, 958–961.
 40. Kraulis, P.J. (1991). MOLSCRIPT – a program to produce both detailed and schematic plots of protein structures. *J. Appl. Crystallogr.* **24**, 946–950.
 41. Merritt, E.A., and Murphy, M.E.P. (1994). Raster 3D Version 2.0 - a program for photorealistic molecular graphics. *Acta Crystallogr. D* **50**, 869–873.
 42. Nicholls, A., Sharp, K., and Honig, B. (1991). Protein folding and associations: insights from the interfacial and thermodynamic properties of the hydrocarbons. *Proteins Struct. Funct. Gen.* **11**, 281–296.
 43. Wallace, A.C., Laskowski, R.A., and Thornton, J.M. (1995). Ligplot – a program to generate schematic diagrams of protein ligand interactions. *Protein Eng.* **8**, 127–134.

Accession Numbers

The coordinates for the structures of the *A. fulgidus* FeR and its complex with NADP⁺ will be deposited in the RCSB Protein Data Bank for release upon publication (accession numbers 110R and 110S).